Available online at www.sciencedirect.com

jmr&t Journal of Materials Research and Technology

journal homepage: www.elsevier.com/locate/jmrt

Original Article

Evaluating recycling potential of waste alumina powder for ceramics production using response surface methodology

Milan Vukšić [a,*], Irena Žmak [a], Lidija Ćurković [a], Danko Ćorić [a], Petra Jenuš [b], Andraž Kocjan [b]

[a] Faculty of Mechanical Engineering and Naval Architecture, University of Zagreb, Ivana Lučića 5, Zagreb, 10000, Croatia

[b] Department for Nanostructured Materials, Jožef Stefan Institute, Jamova cesta 39, Ljubljana, 1000, Slovenia

ARTICLE INFO

Article history:
Received 3 September 2020
Accepted 18 January 2021
Available online 23 January 2021

Keywords:
Alumina
Recycling
Sintering
Mechanical properties

ABSTRACT

The generated process losses such as broken ware from shaping, if not recycled internally, are considered as waste. Furthermore, the collected process losses are provided to external recycling companies or waste disposal facilities. This study investigated the recycling potential of waste alumina powder, which was accumulated during industrial machining of the ceramic green body. The samples containing up to 20 dwb. % (dwb – weight amounts based on dry matter) of powdered waste alumina were prepared by slip casting method and conventionally sintered at various sintering conditions according to Box-Behnken design. Sintered samples were characterized for density, microstructure, hardness, and indentation fracture toughness and compared with samples made of pure commercial alumina. The study shows that the addition of waste alumina up to 20 dwb. % sintered at higher sintering temperature with dwell time 1–3 h did not negatively affect the hardness, nor the indentation fracture toughness of the sintered samples. The enabled recycling potential of waste alumina powder can have direct positive environmental impact, although economic benefits cannot be ignored.

1. Introduction

Alumina is a well-known and widely used family of technical ceramics owing to remarkable combination of properties including high strength and hardness, thermal stability, wear resistance, as well as the chemical stability at elevated temperatures. Ruys [1] described production of alumina, which is primarily derived from bauxite ore through the Bayer process. Currently, bauxite is the only alumina precursor on a commercial scale. Furthermore, Sverdrup et al. [2] stated that the average price of aluminum has remained constant despite increasing production outputs throughout the 20th century to the present, which is the consequence of high demand.

* Corresponding author.
E-mail address: milan.vuksic@fsb.hr (M. Vukšić).

https://doi.org/10.1016/j.jmrt.2021.01.064

The European Commission recently implemented an ambitious Action Plan related to Circular Economy. According to Action Plan the overwhelming legislative revision on waste management was designed to boost the transition towards a circular economy. New legislative proposals implemented in waste management set decisive goals for the waste reduction in general by promoting the use of secondary materials as a substitute for primary resources [3]. Morseletto [4] pointed out that these solutions allow companies to reduce disposal costs and generate added value by transforming waste materials, which had previously made costs for them, into secondary raw materials [4]. Industrial ceramic processing inevitably yields process losses such as broken ware from green and post sintering shaping, during drying process, firing the refractory material, different kinds of sludge, generated dust, and used plaster molds. Some of the generated process losses can be recycled and reused internally within the plant according to provided product specifications or process conditions; otherwise, remaining materials are considered as waste and then provided to external recycling companies or waste disposal facilities [5]. Martins et al. [6] considering sustainable development emphasized that not only the steady consumption of raw materials is alarming because of the natural resources depletion, but also causes environmental and economic impacts.

The waste alumina powder used in this study was generated during the ceramic production process. In the first step, a spray-dried thermally reactive alumina powder which contains up to 5 wt. % of organic binder was pressed at high pressure into a pre-designed mold to form a raw shape. After the pressing, the ceramic compact was subjected to the green machining as closely as possible to desired final dimensions. The green machining is a far more economically favorable than post-machining after the sintering process. The broken ware generated during this forming step was collected by industrial dust sucking machine into bags for further storage. The practical implementation of circular economy in ceramic manufacturing is gaining more interest by researchers. For instance, Lemougna et al. [7] investigated the recycling possibility of the spodumene generated during lithium production as a secondary raw material in ceramic production. The developed porcelain material exhibited satisfactory properties in comparison with the reference porcelain. The necessity of using sustainable and efficient materials boost similar studies. Glymond et al. [8] reused furnace bottom ash from coal power station as a primary raw material with 20 wt. % glass addition to produce ceramic material. This composition sintered at 980 °C showed adequate properties although additional data as density and hardness characterization were needed. Gouvêa et al. [9] investigated the implementation of bone ash as a sintering additive for porcelain production. The addition up to 5 wt. % calcined bovine bone resulted with increased consolidation rate in the sintering range 1100 °C–1400 °C.

The goal of this study was to check the possibility of recycling broken ware from shaping alumina compacts as secondary raw material to produce high-quality technical ceramics. Therefore, the design of experiments by Box-Behnken (BBD) was applied to determine the effect of the sintering regime (temperature, dwell time) and the addition of waste alumina powder on the density, hardness, as well as the indentation fracture toughness of the sintered as-prepared alumina ceramics. Also, the microstructure of the thermally etched samples with various weight content additions of waste alumina powder was applied to study the impact on the morphology of the sintered samples. The samples without the addition of waste alumina powder were taken as a reference point for the comparison.

2. Materials and methods

2.1. Starting alumina powders

The waste alumina powder, which is generated during machining of alumina green compacts and high-purity 99.9 wt. % alumina powder (α-Al_2O_3, Alcan Chemicals, USA), were used as starting materials. The chemical composition of used alumina powders is showed in Table 1.

The particle size distribution (PSD) of both powders was determined by applying the laser diffraction method (Horiba LA-920, Kyoto, Japan). Prior to the measurements, the aqueous dispersions containing pure and waste alumina powder were dispersed separately using the Dolapix® (Zschimmer & Schwarz GmbH Co., Germany) as a dispersant agent.

The powder X-ray diffraction analysis (AXS D4 Endeavor, Bruker AXS GmbH, Germany) was conducted on as received starting alumina powders for secondary phases or impurities. The measurement conditions were as follows: CuKα radiation at ambient temperature, the 2θ range from 20° to 80°, step size 0.04, and acquisition time per a channel of 3 s. The Raman spectra of alumina powders were recorded on a Raman spectrometer (NTegra Spectra II, NT-MDT, Russia) using a 633 nm laser.

2.2. Suspension preparation and sintering

The different weight ratios of alumina powders were dispersed in an aqueous medium to form a suspension with a total solid loading of 70 wt. % using 0.1 wt. % Tiron® (Sigma–Aldrich Chemie GmbH, Germany) as the dispersant.

Table 1 – Chemical composition of pure and waste alumina powder.

Powder	Component	MgO	Fe_2O_3	SiO_2	Na_2O	CaO	Al_2O_3
Pure	wt. %	0.06	0.02	0.02	0.05	0.01	99.85
Waste[a]	wt. %	0.10	0.02	0.02	0.08	0.03	99.70

[a] Used in the first cycle of manufacturing.

Table 2 – Three independent factors varied at three levels according to BBD.

Run	Temperature (°C)		Dwell time (h)		Waste alumina powder (% dwb.)	
	Coded	Actual	Coded	Actual	Coded	Actual
1	0	1500	0	2	0	10
2	0	1500	−1	1	−1	0
3	0	1500	1	3	1	20
4	0	1500	0	2	0	10
5	−1	1400	0	2	1	20
6	1	1600	0	2	−1	0
7	−1	1400	1	3	0	10
8	−1	1400	−1	1	0	10
9	0	1500	0	2	0	10
10	0	1500	−1	1	1	20
11	1	1600	1	3	0	10
12	0	1500	1	3	−1	0
13	−1	1400	0	2	−1	0
14	1	1600	0	2	1	20
15	1	1600	−1	1	0	10

According to BBD (Table 2), the three different compositions were prepared by using the slip casting method: to the pure (commercial) alumina powder various percentages (0, 10, and 20 dwb. %) of waste alumina powder were added. The prepared suspensions were mixed in a planetary ball mill (PM100, Retsch GmbH, Germany) with a high purity alumina balls at a speed rate of 300 rpm for 90 min. Additionally, the suspension was exposed to an ultrasonic treatment in the duration of 15 min by utilizing ultrasonic bath (B 220, Branson Ultrasonics Corp., USA) to achieve better homogeneity and remove the remaining air bubbles from suspension, followed by slip casting into cubical gypsum molds (21 mm × 21 mm × 21 mm). The minimum of three prepared green body samples were dried for 24 h at ambient temperature for each experimental run. After drying the green samples were sintered by using an electric furnace (LHT 04/18 electric furnace, Nabertherm GmbH, Bremen, Germany). The sintering regime was programmed to apply the heating rate of 3 °C/min until 500 °C and the dwell time of 30 min to remove all organics from the samples. The same heating rate was applied to achieve the targeted sintering temperature of 1400–1600 °C in the air atmosphere for 1–3 h, according to BBD, as showed in Table 2. A comparably low heating rate of 3 °C/min was chosen in this study, because preliminary testing had shown that a further increase in heating rate up to 10 °C/min negatively affects the quality of sintered samples.

2.3. *Microstructural and mechanical characterization*

Samples obtained after sintering were characterized for density, microstructure, hardness, and indentation fracture toughness. Sample's density was determined by the Archimedes principle using density meter (JP703C, Mettler-Toledo GmbH, Switzerland). Dhuban et al. [10] reported the alumina theoretical density of 3.98 g/cm^3, which was used for the relative density calculations of sintered alumina samples. The sintered samples were prepared according to standard ceramographic procedure, which includes grinding and polishing for microstructure investigation and mechanical tests. The microstructure of selected sintered alumina samples was studied by utilizing a FE-SEM (JSM-7600F, Jeol Inc., Japan). The samples were polished and thermally etched for 30 min at a temperature 50 °C lower than their sintering temperature. Several SEM images were taken from the center to the periphery of the sample surface and processed in order to determine the average grain size. Seidel et al. [11] proposed the application of the linear intercept technique for measuring the average grain diameter when there are at least 100 grains/per sample analysis, so this method was applied for computing the average alumina grain size.

The testing of mechanical properties such as the hardness and the following calculation of the indentation fracture toughness were conducted by at least 5 repetitions per sample. The Vickers indentation fracture toughness (VIF) method was applied on sintered and polished samples. The method includes the length measurement of cracks emanating from the hardness impression as a result of the applied load. Hardness and indentation fracture toughness measurements were performed using HV30, i.e. under the load of 294.2 N during 15 s. The hardness impressions were made by utilizing a hardness tester (5030 TKV, Indentec Hardness Testing Machines Ltd., UK). After unloading, the hardness impression diagonal and the formed cracks were measured utilizing an optical microscope (GX51F-5, Olympus Imaging Corp., Japan). Based on Nastic et al. [12] research, Tanaka's Eq. (1) was selected as a suitable method to determine the indentation fracture toughness. The indentations crack lengths (c), measured from the center of the hardness impressions, the applied load (P), and the empirical constant of 0.0725, were used to compute the indentation fracture toughness (K_{IC}) by the direct crack measurement applying the median crack model:

$$K_{IC} = 0.0725\left(P / c^{3/2}\right) \quad (1)$$

2.4. *Box-Behnken experimental design*

The response surface methodology (RSM) represents a collection of various statistical and mathematical methods which can be used for the design of experiments, developing models, estimating the process parameters effects in the selected range, and obtaining the optimum process parameters for the desired responses. BBD is the common design tool of RSM constitutes, which is put to use for the numerical optimization of different chemical and physical processes. Ferreira et al. [13] described the BBD as a globular and rotary design, which involves three interlocking blocks with two level two factors (2^2) factorial designs and a central point limited on the sphere. The number of total experiments (N) required for a BBD experimental design can be calculated according to expression $N = 2n_F\ (n_F\text{-}1) + n_C$, where ($n_F$) is the number of selected factors, and (n_C) is the number of the selected central points. The main limitation of the RSM is that the developed response surface is valid only for studied ranges of selected factors.

The study presented in this paper employed a BBD to determine the effects of three independent factors, i.e., A-the amount of waste alumina powder (0–20 dwb. %), B-the

sintering temperature (1400–1600 °C) and C-the dwell time (1–3 h) on the following responses: density, Vickers hardness, as well as the indentation fracture toughness of the sintered samples. As suggested by Raymond H. Myers et al. [14], the BBD method was chosen because it provides a mathematical model to estimate the interaction between independent factors on monitored responses with a small number of experiments. The generated design consisted of 15 experiments in total, including three iterations at the center point. The Design-Expert® software (ver. 11.1.2) was implemented for designing of experiments, model establishing, and statistical data analysis. Table 2 shows the three levels of each monitored factor, which were coded as high (1), middle (0), and low (−1).

3. Results and discussion

3.1. *Alumina powder properties*

The cumulative curve and the PSD of both alumina powders expressed on the volume basis is shown in Fig. 1. The size range of the waste alumina powder is much broader compared to the size range of pure alumina powder. The multimodal PSD was observed for waste alumina particles as a result of the green machining. The particle size range of waste alumina powder was from 0.2 to 214.0 μm (Fig. 1B), while the particle size range of pure alumina was from 0.2 to 11.0 μm (Fig. 1A). The mean values of pure and waste alumina particle diameter were 1.31 ± 1.26 and 3.35 ± 1.03 μm, respectively. The determined specific surface area values were 3.42 m^2/g and 7.57 m^2/g for pure and waste alumina powder, respectively, as determined by using the Brunauer–Emmett–Teller (BET) nitrogen adsorption analyzer (Quantachrome Nova 2000e, Anton Paar QuantaTec Inc., Austria). The PSD with the maximum addition of waste alumina powder after the 90 min of ball milling at 300 rpm was also investigated: the particle size ranged from 0.2 to 4.5 μm (Fig. 1C), mean value 0.825 ± 0.48 μm and surface area 4.65 m^2/g were detected for the alumina powder mixture.

Raman spectra and XRD diffractograms of alumina powders are shown in Fig. 2. The presence of the corundum (α-alumina) was confirmed, while there was no second phase nor significant impurities present (Fig. 2A). In addition, some peak patterns obtained on waste alumina powder were slightly lower and wider compared to the patterns of pure alumina powder. Scardi and Leoni [15] noticed the effect of grain size and size distribution on the diffraction patterns, so the slight difference between the intensity and shape of peaks observed in Fig. 2A can be explained by the broader PSD of waste alumina powder (Fig. 1B).

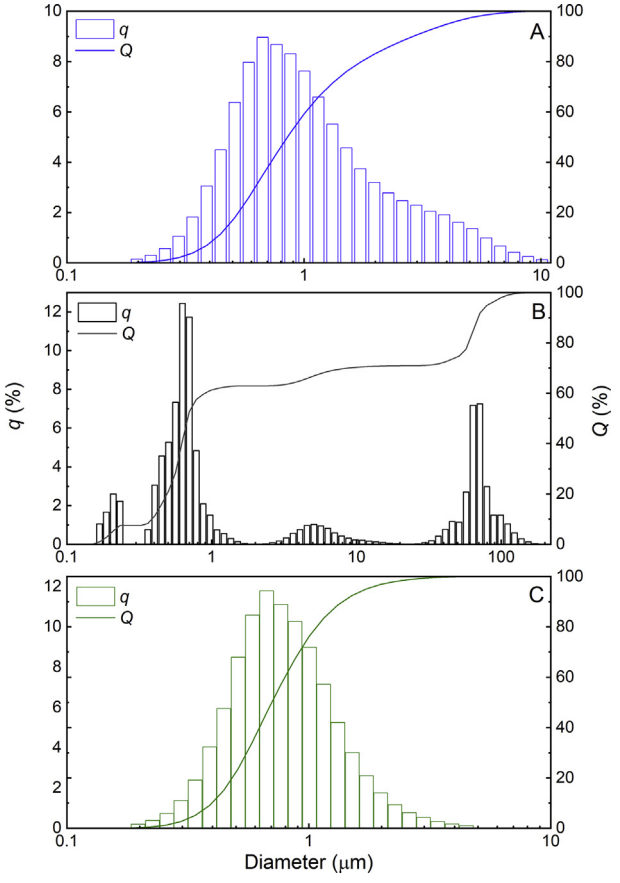

Fig. 1 – The particle size distribution (*q*) with the cumulative curve (Q) of A) pure alumina powder, B) waste alumina powder, C) alumina powder mixture (4:1) after ball milling.

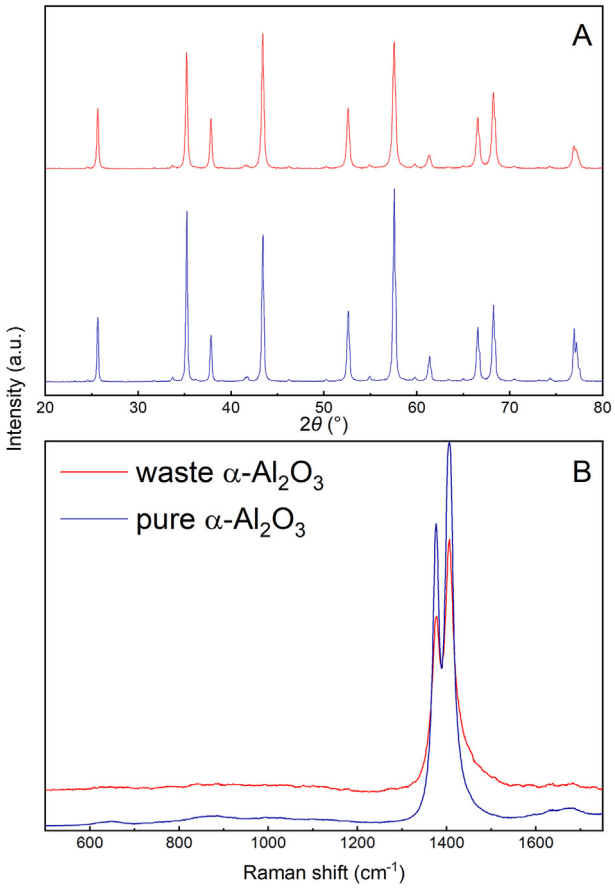

Fig. 2 – A) XRD patterns, B) Raman spectra of waste and pure alumina powder.

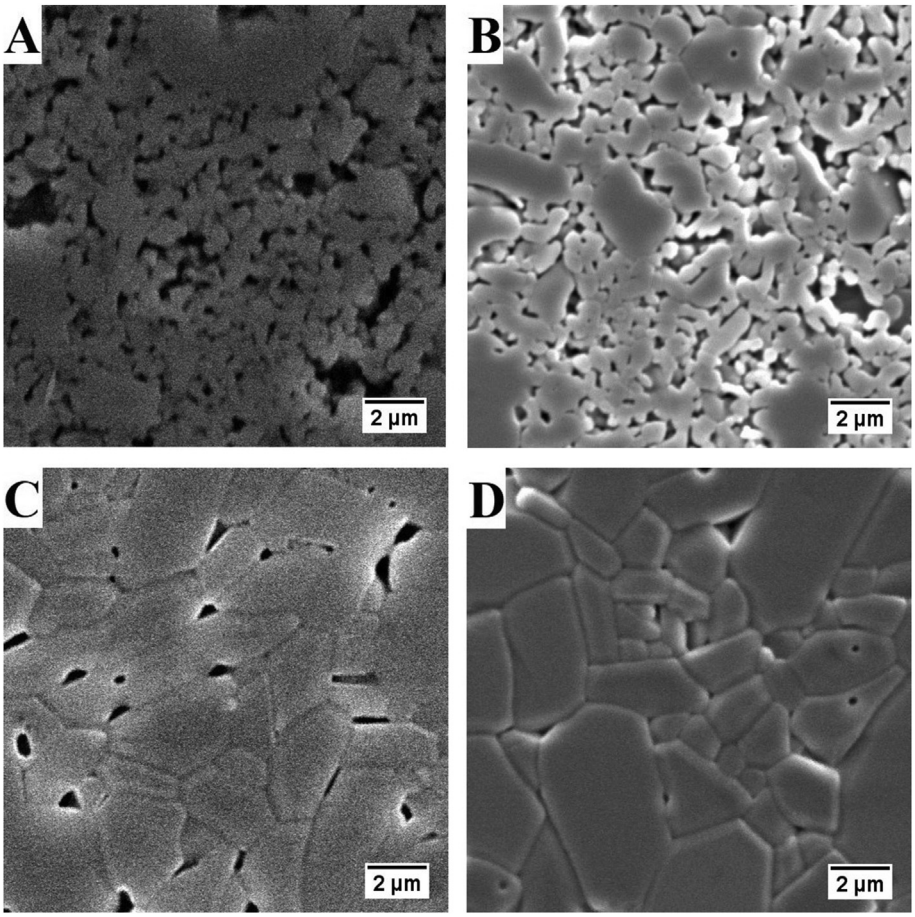

Fig. 3 – FE-SEM images of alumina surface microstructure: A) 1400 °C/0 dwb. %, B) 1400 °C/20 dwb. %, C) 1600 °C/0 dwb. %, D) 1600 °C/20 dwb. %.

The Raman spectrum also demonstrated the presence of corundum (Fig. 2B). The corundum alumina phase had strong Raman peaks at 1375.6 cm^{-1} and 1404.5 cm^{-1} on spectra of both examined alumina powders. The spectrum of pure alumina had a slightly higher intensity $I_{pure\ alumina} = 0.79$ and narrower peak base then the spectrum intensity of the waste alumina powder $I_{waste\ alumina} = 0.74$. As Stolyarov et al. [16] detected on Raman scattering of alumina/graphene nanocomposite that the peak base width is related to the crystallinity and to the degree of disorder, the observed difference in the intensity could be attributed to the degree of disorder in waste alumina powder.

3.2. *Microstructures of sintered alumina*

The microstructures of alumina samples sintered at various sintering temperatures are depicted in Fig. 3. The effect of the sintering temperature, amount of waste alumina, and grain size on the properties of alumina samples is demonstrated in Table 3. The value of dwell time was fixed at 2 h because of the negligible impact on density, hardness, and indentation fracture toughness in the investigated range (see Chapter 3.4.).

At the lowest investigated sintering temperature of 1400 °C, the consolidation process was incomplete therefore the so-called necking between alumina particles can be seen and pronounced grain boundaries were absent as well, as shown in Fig. 3A and 3B. This has been reflected in very low hardness and indentation fracture toughness values (Table 3). The increase in the sintering temperature to 1600 °C, increased the consolidation rate, resulting in distinct and visible grain boundaries. The increase in obtained mechanical properties is also noticed (Table 3). The increasing content of the waste alumina in studied samples resulted in finer microstructure due to the higher amount of MgO (Table 1). Magnesia doping causes a reduction in grain boundary mobility of alumina, resulting with the reduction in alumina grain size at higher sintering temperatures (Fig. 3C and 3D) [17,18]. The addition of 20 dwb. % of waste alumina powder did not negatively affect the obtained density (Table 2) and microstructure of sintered samples (Fig. 3).

3.3. *Response surface regression analysis*

The experimentally obtained response values from the BBD were fitted to the polynomial second-order model to find the most adequate regression equations. In Table 4 the impacts of independent variables on the observed responses are shown. Also, the predicted responses calculated from the empirical equations are indicated for each response. The empirical regression equations which define the relationship of the

Table 3 – Properties of alumina ceramics after sintering process[a].

Sintering temperature (°C)	Amount of waste alumina (dwb. %)	Grain size (μm)	Density (g/cm^3)	Hardness (HV30)	Indentation fracture toughness (MPa m$^{1/2}$)
1400	0	0.87 ± 0.48	3.724 ± 0.013	508.1 ± 7.1	2.06 ± 0.08
1400	20	1.17 ± 0.48	3.781 ± 0.007	515.4 ± 12.0	2.40 ± 0.16
1600	0	2.63 ± 1.24	3.793 ± 0.007	1453.9 ± 23.5	3.28 ± 0.23
1600	20	1.78 ± 1.03	3.818 ± 0.013	1454.7 ± 90.7	4.11 ± 0.22

[a] The ± sign indicates standard deviation.

independent factors for each output are shown in Eqs. (2)–(4). The relationship between the independent factors and density response was described with reduced quadratic model, Eq. (2), while the hardness and the indentation fracture toughness responses were described with linear models, Eqs. (3) and (4).

$$Y_1(\text{Density, g/cm}^3) = -1.0809 + 0.0062 \times A - 0.0035 \times B + 0.0168 \times C - 8 \times 10^{-6} \times A \times C + 9.50 \times 10^{-4} \times B \times C - 1.9692 \times 10^{-6} \times A^2 - 2.37 \times 10^{-4} \times C^2 \quad (2)$$

$$Y_2(\text{Hardness, HV30}) = -6205.1817 + 4.7263 \times A + 27.9 \times B + 4.26 \times C \quad (3)$$

$$Y_3(\text{Indentation fracture toughness, MPa m}^{1/2}) = -7.5842 + 0.0069 \times A - 0.0375 \times B + 0.0176 \times C \quad (4)$$

where:

- A is the sintering temperature (°C),
- B is the dwell time (h),
- C is the addition of waste alumina powder (dwb. %).

In order to determine the significance of the selected model, the Design-Expert® software was applied again. The same software was used to estimate the goodness of fit for the selected model, the coefficient of determination (R^2), and for plotting the response surfaces. The F-test and p-values were obtained by the analysis of variance (ANOVA). Based on these values, the significances of each coefficient in the empirical regression equations were determined. Response plots were generated to visualize the effects of the chosen factors in previously defined range on the monitored responses.

The acceptability of the response surface models was estimated by ANOVA shown in Table 5. The F-test and p-values ($p < 0.05$) were determined for all three obtained models. The F-value of 16.01 and the appropriate $p < 0.001$ suggest that the reduced quadratic model of the density response is highly significant. The F-value 168.13 ($p < 0.0001$) of hardness and F-value 43.40 ($p < 0.0001$) of indentation fracture toughness response data, which were fitted into the linear model also indicated a high level of significance for the employed model. Furthermore, the coefficient of determination (R^2) of the statistical models were as follows: (Y_1) density response 0.9412, (Y_2) hardness response 0.9787 and (Y_3) indentation fracture toughness response 0.9221 suggesting that the obtained models can explain the responses satisfactorily. The "Predicted R^2" values of 0.6827, 0.9566 and 0.8379 are in agreement with the "Adjusted R^2" of 0.8824, 0.9728 and 0.9008, which additionally confirms the predictability of the models.

Table 4 – Monitored responses and predicted data of applied BBD.

Run	Box-Behnken design			Response					
	A temperature	B dwell time	C amount of waste alumina	Density (g/cm^3)		Hardness (HV30)		Indentation fracture toughness (MPa m$^{1/2}$)	
	(°C)	(h)	(dwb. %)	Experimental	Predicted	Experimental	Predicted	Experimental	Predicted
1	1500	2	10	3.819 ± 0.014	3.824 ± 0.191	939.1 ± 13.9	982.6 ± 49.1	2.95 ± 0.22	2.92 ± 0.15
2	1500	1	0	3.793 ± 0.001	3.785 ± 0.189	865.7 ± 18.3	912.1 ± 45.6	3.05 ± 0.11	2.79 ± 0.14
3	1500	3	20	3.832 ± 0.007	3.835 ± 0.192	1043.4 ± 16.5	1053.1 ± 52.7	2.88 ± 0.08	3.06 ± 0.15
4	1500	2	10	3.814 ± 0.011	3.824 ± 0.191	1015.5 ± 32.6	982.6 ± 49.1	2.93 ± 0.12	2.92 ± 0.15
5	1400	2	20	3.781 ± 0.007	3.787 ± 0.189	515.4 ± 12.0	552.6 ± 27.6	2.40 ± 0.16	2.41 ± 0.12
6	1600	2	0	3.793 ± 0.017	3.791 ± 0.190	1453.9 ± 23.5	1412.6 ± 70.6	3.28 ± 0.23	3.44 ± 0.17
7	1400	3	10	3.799 ± 0.010	3.789 ± 0.189	539.2 ± 6.5	537.9 ± 26.9	2.38 ± 0.14	2.19 ± 0.11
8	1400	1	10	3.783 ± 0.003	3.777 ± 0.189	441.5 ± 11.7	482.1 ± 24.1	2.06 ± 0.16	2.27 ± 0.11
9	1500	2	10	3.832 ± 0.020	3.824 ± 0.191	946.8 ± 23.5	982.6 ± 49.1	2.78 ± 0.10	2.92 ± 0.15
10	1500	1	20	3.810 ± 0.014	3.804 ± 0.190	1147 ± 26.8	997.3 ± 49.9	3.16 ± 0.24	3.14 ± 0.16
11	1600	3	10	3.836 ± 0.008	3.832 ± 0.192	1489.7 ± 37.9	1483.1 ± 74.2	3.51 ± 0.20	3.58 ± 0.18
12	1500	3	0	3.777 ± 0.006	3.778 ± 0.189	992 ± 34.8	967.9 ± 48.4	2.75 ± 0.10	2.71 ± 0.14
13	1400	2	0	3.724 ± 0.013	3.732 ± 0.187	508.1 ± 7.1	467.4 ± 23.4	2.06 ± 0.16	2.05 ± 0.10
14	1600	2	20	3.818 ± 0.013	3.813 ± 0.191	1454.7 ± 90.7	1497.8 ± 74.9	4.11 ± 0.22	3.79 ± 0.19
15	1600	1	10	3.810 ± 0.018	3.820 ± 0.191	1386.9 ± 12.9	1427.3 ± 71.4	3.55 ± 0.17	3.66 ± 0.18

*The ± sign indicates standard deviation.

Table 5 – ANOVA results for fitted regression models of monitored responses.

Source	Density				Hardness				Fracture toughness			
	Sum of squares	F-value	p-value		Sum of squares	F-value	p-value		Sum of squares	F-value	p-value
Model	0.0108	16.01	0.0008	**Model**	1.808×10^6	168.13	<0.0001	**Model**	4.11	43.40	<0.0001
A	0.0036	37.57	0.0005	**A**	1.787×10^6	498.61	<0.0001	**A**	3.85	121.97	<0.0001
B	0.0003	3.00	0.1271	**B**	6227.28	1.74	0.2142	**B**	0.0113	0.3564	0.5626
C	0.0030	30.83	0.0009	**C**	14518.08	4.05	0.0693	**C**	0.2485	7.87	0.0171
AC	0.0003	2.66	0.1468								
BC	0.0004	3.75	0.0939								
A^2	0.0014	14.98	0.0061								
C^2	0.0021	21.68	0.0023								
Residual	0.0007	**Lack of fit**	0.5234	**Residual**	39423.64	**Lack of fit**	0.3451	**Residual**	0.3473	**Lack of fit**	0.2051
Pure error	0.0002	R^2	0.9412	**Pure error**	3538.65	R^2	0.9787	**Pure error**	0.0173	R^2	0.9221
Adequate Precision	14.3751	**Adjusted R^2**	0.8824	**Adequate Precision**	33.3319	**Adjusted R^2**	0.9728	**Adequate Precision**	18.9642	**Adjusted R^2**	0.9008
C.V. %	0.2580	**Predicted R^2**	0.6827	**C.V. %**	6.09	**Predicted R^2**	0.9566	**C.V. %**	6.08	**Predicted R^2**	0.8379

The model's "Adequate Precision" ratio represents the ratio between the signal and the noise, and its values were 14.38, 33.33 and 18.96. The ratio >4 is considered as desirable ratio which suggest that the all suggested models can be applied to the entire design area. As presented by Bouriche et al. [19], the "Lack of Fit Test" was shown as not significant according to the obtained p-values > 0.05, which indicates that all developed models fit the data well. Hence, the response surface models developed with the purpose of describing the influence of dwell time, sintering temperature and amount of waste alumina powder on density, hardness, and indentation fracture toughness were deduced to be satisfactory.

3.4. *Interactive effects of monitored factors on responses*

Table 5 shows the effects of independent variables on observed responses throughout p-values. Chan et al. [20] used the following criterion, which was chosen in the presented study as well. If the p-values are >0.1, it means that the model factors were not significant, while p-values < 0.05 indicate that the model factors were significant for the monitored responses.

Considering the reduced quadratic regression model of density response, it is noticeable that the sintering temperature and the amount of waste alumina powder added to starting powder formulation showed the highly significant effect ($p << 0.05$) on density. The density values of sintered alumina samples had an increasing trend when the sintering temperature was increased, as a result of pore elimination during the final sintering stage. The highest density was achieved at the sintering temperature of 1600 °C. The positive effect of waste alumina on the density is explained with higher dispersant content in the alumina suspensions with present waste alumina powder compared to pure alumina suspensions. The organic additives had remained in waste alumina powder after the first cycle of industrial alumina ceramics production, i.e. green machining. Also, the slightly higher content of sodium was noticed in waste alumina powder (Table 1), which can facilitate the sintering process [21].

The dwell time in the investigated range did not show a significant impact ($p > 0.10$) on the density of the sintered alumina samples (Table 5). In the conducted study, the sample containing 10 dwb. % of waste alumina powder, sintered at 1600 °C for dwell time of 3 h, achieved the highest density 3.836 g/cm^3 (relative density ≈ 97%) of all investigated compositions (Table 4). Fig. 4A plots the response surface graph indicating the dependence of density on the sintering temperature and the waste alumina amounts.

The next studied response was the hardness. The regression analysis of experimental data resulted in a linear correlation between independent factors and the hardness response, with the most significant factor ($p << 0.05$) being the sintering temperature. When the sintering temperature was increased from 1400 °C to 1600 °C, the hardness values followed a linear increase. This trend can be explained by the consolidation process and by the change in average grain size (Table 3) as a result of higher sintering temperatures. Rice et al. [22] investigated the correlation between hardness and grain size for ceramic materials, and it was

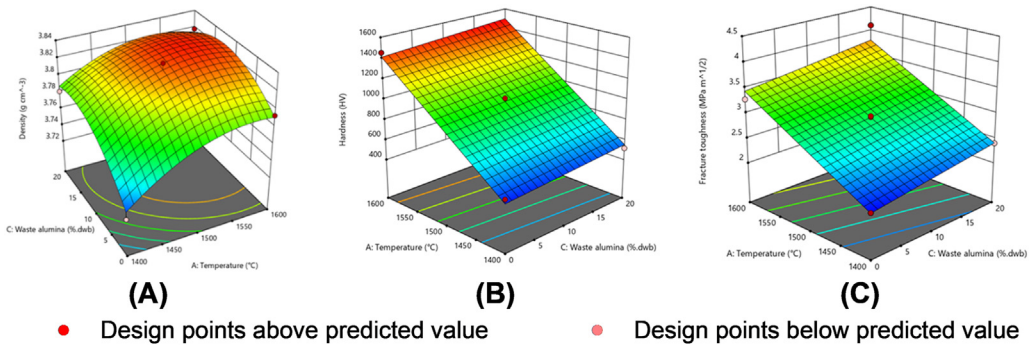

Fig. 4 – Response surface charts: influence of sintering temperature and waste alumina content on: A) density, B) hardness, C) indentation fracture toughness.

determined that in finer ceramic microstructure, the measured hardness of oxide ceramics demonstrates an increase in hardness with decreasing the grain size. Rice et al. [22] also found an exponential decrease in hardness with the increasing porosity. In this study, the remaining independent variables (dwell time and waste content) did not show a significant effect ($p > 0.05$) on the obtained hardness of sintered samples. The values of hardness increased very slightly by the addition of a higher content of waste alumina powder, while changes in hardness are not observed with the change of dwell time. In Fig. 4B, a response surface graph that depicts the influence of the sintering temperature and amount of waste alumina on the hardness values of sintered samples is shown.

The final response, i.e. the indentation fracture toughness, was also fitted into the linear regression model, similar to the hardness response. The model also demonstrated a linear relationship between the chosen factors on the indentation fracture toughness of the sintered samples. The significant factor ($p << 0.05$) was the sintering temperature. The values of the indentation fracture toughness calculated by Tanaka's equation varied in the range from 2.06 ± 0.16 to 4.11 ± 0.22 MPa $m^{1/2}$. The slight but constant linear increase of indentation fracture toughness values was observed when the sintering temperature was increased in the selected range, starting from 1400 to 1600 °C. The fracture toughness mechanism for alumina ceramics were evaluated by many researchers. Yao et al. [23] reported that the bridging effect is weak in comparison with the grain boundaries weakening effect. Koyama et al. [24] noticed the impact of slight increase in grain size onto increasing the indentation fracture energy. These described mechanisms may be applied to the explanation of the observed increasing fracture toughness, presented in this study. The amount of waste alumina in the investigated range demonstrated a weak impact ($p > 0.01$) on the increase of indentation fracture toughness. The increase of dwell time from 1 to 3 h did not affect ($p >> 0.10$) the indentation fracture toughness. Fig. 4C shows a significant improvement in indentation fracture toughness by increasing the sintering temperature, while the waste content did not show a strong effect.

4. Conclusions

The effect of the sintering temperature, amount of waste alumina powder, and dwell time on the density, the hardness, and indentation fracture toughness were investigated to assess the recycling potential of waste alumina as secondary raw material. The obtained regression models confirmed that the addition of waste alumina powder did not negatively affect the observed responses. On the contrary, the addition of waste alumina powder slightly increased the density, which consequently caused also a positive effect on the hardness and indentation fracture toughness of obtained alumina samples. Such an effect can be explained by the industrial sintering additives, already present in the waste alumina powder, which had remained from the first production cycle. The sintering temperature by the increase to 1600 °C demonstrated a strong positive effect on mechanical properties. For the investigated range from 1 to 3 h, the dwell time did not significantly affect any of the monitored responses. Based on the investigated ranges, following sintering conditions were suggested: 1600 °C, 3 °C/min, and 1 h. The collected and processed results indicate the feasibility of reusing the waste alumina powder up to 20 dwb. % as a secondary raw material limited to slip casting technique.

Declaration of Competing Interest

The authors declare that they have no known competing financial interests or personal relationships that could have appeared to influence the work reported in this paper.

Acknowledgments

This work was supported by the Croatian Science Foundation under the project [IP-2016-06-6000]: Monolithic and Composite Advanced Ceramics for Wear and Corrosion Protection (WECOR) and by the Slovenian-Croatian Bilateral project [BI-HR/18-19-048], 2018–2019; the Slovenian National Research Programme [P2-0087]: Ceramics and complementary materials for advanced engineering and biomedical applications.

REFERENCES

[1] Ruys A. 3 - refining of alumina: the Bayer process. In: Ruys A, editor. Alumina ceram. Woodhead Publishing; 2019. p. 49–70. https://doi.org/10.1016/B978-0-08-102442-3.00003-8.

[2] Sverdrup HU, Ragnarsdottir KV, Koca D. Aluminium for the future: modelling the global production, market supply, demand, price and long term development of the global reserves. Resour Conserv Recycl 2015;103:139–54. https://doi.org/10.1016/j.resconrec.2015.06.008.

[3] Closing the loop—an EU action plan for the circular economy (COM/2015/0614). 2015. Available online: https://eur-lex.europa.eu/legal-content/EN/TXT/?uri=CELEX:52015DC0614. [Accessed 5 August 2020].

[4] Morseletto P. Targets for a circular economy. Resour Conserv Recycl 2020;153:104553. https://doi.org/10.1016/j.resconrec.2019.104553.

[5] The European commission's BREF document on the ceramic manufacturing industry (CER). 2007. Available online: https://eippcb.jrc.ec.europa.eu/sites/default/files/2019-11/cer_bref_0807.pdf. [Accessed 5 August 2020].

[6] Martins VWB, Rampasso IS, Anholon R, Quelhas OLG, Leal Filho W. Knowledge management in the context of sustainability: literature review and opportunities for future research. J Clean Prod 2019;229:489–500. https://doi.org/10.1016/j.jclepro.2019.04.354.

[7] Lemougna PN, Yliniemi J, Ismailov A, Levanen E, Tanskanen P, Kinnunen P, et al. Spodumene tailings for porcelain and structural materials: effect of temperature (1050–1200 °C) on the sintering and properties. Miner Eng 2019;141:105843. https://doi.org/10.1016/j.mineng.2019.105843.

[8] Glymond D, Roberts A, Russell M, Cheeseman C. Production of ceramics from coal furnace bottom ash. Ceram Int 2018;44:3009–14. https://doi.org/10.1016/j.ceramint.2017.11.057.

[9] Gouvêa D, Tisse Kaneko T, Kahn H, de Souza Conceição E, Antoniassi JL. Using bone ash as an additive in porcelain sintering. Ceram Int 2015;41:487–96. https://doi.org/10.1016/j.ceramint.2014.08.096.

[10] Dhuban SB, Ramesh S, Tan CY, Wong YH, Johnson Alengaram U, Ramesh S, et al. Sintering behaviour and properties of manganese-doped alumina. Ceram Int 2019;45:7049–54. https://doi.org/10.1016/j.ceramint.2018.12.207.

[11] Seidel J, Claussen N, Rödel J. Reliability of alumina ceramics: effect of grain size. J Eur Ceram Soc 1995;15:395–404. https://doi.org/10.1016/0955-2219(95)91430-V.

[12] Nastic A, Merati A, Bielawski M, Bolduc M, Fakolujo O, Nganbe M. Instrumented and Vickers indentation for the characterization of stiffness, hardness and toughness of zirconia toughened Al_2O_3 and SiC armor. J Mater Sci Technol 2015;31:773–83. https://doi.org/10.1016/j.jmst.2015.06.005.

[13] Ferreira SLC, Bruns RE, Ferreira HS, Matos GD, David JM, Brandão GC, et al. Box-Behnken design: an alternative for the optimization of analytical methods. Anal Chim Acta 2007;597:179–86. https://doi.org/10.1016/j.aca.2007.07.011.

[14] Myers Raymond H, Anderson-Cook Christine M, M DC. Response SurfaceMethodology: process and product optimization using designed experiments. 4th ed. Hoboken, New Jersey: Wiley; 2016.

[15] Scardi P, Leoni M. Diffraction line profiles from polydisperse crystalline systems. Acta Crystallogr A 2001;57:604–13. https://doi.org/10.1107/S0108767301008881.

[16] Stolyarov VV, Frolova AV, Sudzhanskaya IV. Dielectric properties of nanocomposite ceramics Al_2O_3/graphene processed by spark plasma sintering. Ceram Int 2020;46:6920–5. https://doi.org/10.1016/j.ceramint.2019.11.188.

[17] Dillon SJ, Tang M, Carter WC, Harmer MP. Complexion: a new concept for kinetic engineering in materials science. Acta Mater 2007;55:6208–18. https://doi.org/10.1016/j.actamat.2007.07.029.

[18] Bennison SJ, Harmer MP. Effect of magnesia solute on surface diffusion in sapphire and the role-of magnesia in the sintering of alumina. J Am Ceram Soc 1990;73:833–7. https://doi.org/10.1111/j.1151-2916.1990.tb05122.x.

[19] Bouriche S, Cózar-Bernal MJ, Rezgui F, Rabasco Álvarez AM, González-Rodríguez ML. Optimization of preparation method by W/O/W emulsion for entrapping metformin hydrochloride into poly (lactic acid) microparticles using Box-Behnken design. J Drug Deliv Sci Technol 2019;51:419–29. https://doi.org/10.1016/j.jddst.2019.03.011.

[20] Chan Y Ten, Tan MC, Chin NL. Application of Box-Behnken design in optimization of ultrasound effect on apple pectin as sugar replacer. LWT 2019;115:108449. https://doi.org/10.1016/j.lwt.2019.108449.

[21] Louet N, Gonon M, Fantozzi G. Influence of the amount of Na_2O and SiO_2 on the sintering behavior and on the microstructural evolution of a Bayer alumina powder. Ceram Int 2005;31:981–7. https://doi.org/10.1016/j.ceramint.2004.10.013.

[22] Rice R, Wu C, Boichelt F. Hardness–grain-size relations in ceramics. J Am Ceram Soc 2005;77:2539–53. https://doi.org/10.1111/j.1151-2916.1994.tb04641.x.

[23] Yao W, Liu J, Holland TB, Huang L, Xiong Y, Schoenung JM, et al. Grain size dependence of fracture toughness for fine grained alumina. Scr Mater 2011;65:143–6. https://doi.org/10.1016/j.scriptamat.2011.03.032.

[24] Koyama T, Nishiyama A, Niihara K. Effect of grain morphology and grain size on the mechanical properties of Al_2O_3 ceramics. J Mater Sci 1994;29:3949–54. https://doi.org/10.1007/BF00355953.